

#### **OPEN ACCESS**

EDITED BY
Dongfeng Xie,
Zhejiang Institute of Hydraulics & Estuary,
China

REVIEWED BY
Guoxiang Wu,
Ocean University of China, China
Rui Yuan,
Shanghai Maritime University, China
Jieping Tang,
Guangdong Ocean University, China

\*CORRESPONDENCE Feng Liu Iuf53@mail.sysu.edu.cn

RECEIVED 01 September 2025 ACCEPTED 29 September 2025 PUBLISHED 16 October 2025

#### CITATION

Wang P, Hong L, Lin J, Liang H, Li H, Tan C, Chen H and Liu F (2025) Investigating morphological effects of estuarine channel branching on saline water intrusion: a case study of Modaomen Estuary. *Front. Mar. Sci.* 12:1696630. doi: 10.3389/fmars.2025.1696630

#### COPYRIGHT

© 2025 Wang, Hong, Lin, Liang, Li, Tan, Chen and Liu. This is an open-access article distributed under the terms of the Creative Commons Attribution License (CC BY). The use, distribution or reproduction in other forums is permitted, provided the original author(s) and the copyright owner(s) are credited and that the original publication in this journal is cited, in accordance with accepted academic practice. No use, distribution or reproduction is permitted which does not comply with these terms.

# Investigating morphological effects of estuarine channel branching on saline water intrusion: a case study of Modaomen Estuary

Pu Wang<sup>1,2</sup>, Liang Hong<sup>1,2</sup>, Juli Lin<sup>1,2</sup>, Hongyue Liang<sup>1,2</sup>, Haiwei Li<sup>1</sup>, Chao Tan<sup>3</sup>, Hui Chen<sup>3</sup> and Feng Liu<sup>1,2\*</sup>

<sup>1</sup>Institute of Estuarine and Coastal Research, School of Ocean Engineering and Technology, Sun Yat-Sen University, Guangzhou, China, <sup>2</sup>Guangdong Provincial Key Laboratory of Information Technology for Deep Water Acoustics, Guangzhou, China, <sup>3</sup>Guangdong Research Institute of Water Resources and Hydropower, Guangzhou, China

Within the context of global change, morphological evolution in estuary regions and the related effects on water resource safety are key concerns for the sustainable management of river deltas. Channel branching controls the morphological evolution patterns and sedimentary regime in river deltas and generally occurs in response to natural conditions and human activities. In this study, we focused on the impacts of channel branching on saline water intrusion in the Modaomen Estuary in China. The riverine discharge through the Modaomen Estuary supplies freshwater source for the Guangdong- Hong Kong- Macao Greater Bay Area; and morphological evolution greatly affects saline water intrusion in this region, posing a threat to freshwater security. In this study, we constructed an idealized model with a prototype of Modaomen Estuary while considering single and double channels, to explore the impacts of channel branching on saline water intrusion in estuaries. The results indicated that channel branching greatly influenced the morphological structure of the mouth bar in the estuary. The magnitude of saline water intrusion occurred more significantly during the neap tide than spring tide in both the single- and double-channel simulations. Channel branching exhibited different effects on the saline water intrusion during the spring and neap tides, by affecting the estuarine dynamics and circulation. Furthermore, the mouth bar exerted a 'blocking effect' on the intrusion and recession of saline water. Overall, our study presents scientific guidelines for estuarine regulation projects to ensure water resource safety and promote effective estuarine management.

#### KEYWORDS

morphological structure, mouth bar, saline water intrusion, estuarine dynamic, estuarine environment

#### 1 Introduction

Large populations inhabit the coastal areas and river delta regions in the world, which is transition area between land and ocean. Hence, the maintenance of freshwater sources is crucial for ensuring sustainable development. Therefore, freshwater security is a major concern in coastal management, and maintains sustainable development of estuarine environment. Climate change and human activities (e.g. sea-level rise, sand excavation, and channel dredging) exacerbate the issue of saline water intrusion in freshwater sources, posing a threat to freshwater security (Luo et al., 2007; Nicholls and Cazenave, 2010; Costa et al., 2023; Hlaing et al., 2024). Therefore, the patterns and mechanisms of saline water intrusion in estuaries is garnering worldwide attention, particularly in the field of coastal and delta management.

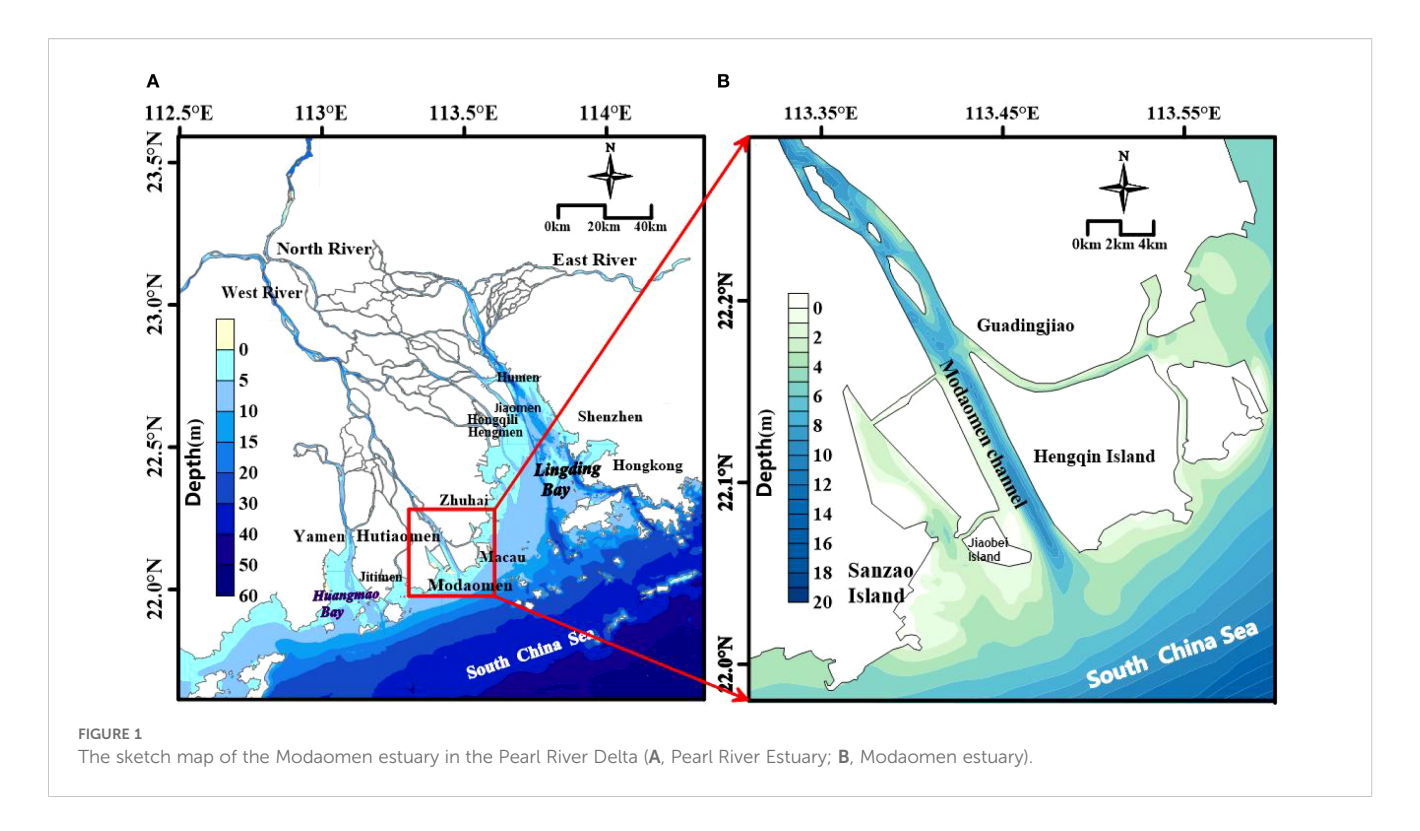
Saline water intrusion in estuaries is characterized by salt transport, which is an important mechanism of material exchange between estuaries and oceans. Salt transport in estuaries is controlled by several physical processes, such as estuarine circulation and tidal pumping (MacCready and Geyer, 2010; Gong et al., 2022b), and is affected by several factors, such as river discharge, tide, wind, and bathymetry (Gong and Shen, 2011; Gong et al., 2022a; Lin et al., 2019; Zhang et al., 2019). Previous studies analyzed the impacts of these factors on saline water intrusion in estuaries. Zhu et al. (2018) indicated that the saltwater intrusion in the Changjiang Estuary was mainly controlled by river discharge and tide and influenced by wind, sea-level rise, river basin characteristics, and estuarine projects. Zhang et al. (2019) analyzed the Yangtze Estuary and revealed that strong northerly and north-easterly winds induced dramatic waterlevel setup, increased the flood-tide current velocities, decreased the ebb tide velocities, and reduced the freshwater inflow into the North Branch of the estuary, thereby increasing the intensity of saline water intrusion. Pokavanich and Guo (2024) reported that the low freshwater discharge, prevailing down-estuary winds and the highest annual sea level were natural causes for the enhancement of estuarine circulation and the greatest saltwater intrusion distance in the Chao Phraya Estuary. In addition, morphological evolution was also an important factor affecting saline water intrusion; however, many studies focused on the impacts of channel incised or deepen on saline water intrusion in the river estuaries and deltas (Wu et al., 2016b; Ralston and Geyer, 2019; Binh et al., 2021). Channel branching often occurs in response to river flooding and human disturbance and influences the morphological structures of shoals and channels (Nguyen et al., 2008). And morphology alterations can greatly affect estuarine processes, including estuarine circulation and tidal pumping (Simpson et al., 1990; Scully and Friedrichs, 2007; Ralston and Geyer, 2019, 2019). However, the impacts of channel branching on saline water intrusion in estuaries remain unexplored, and less knowledge on its influencing mechanism was attained in the previous studies.

In this study, we considered the Modaomen Estuary in the Pearl River Delta in the southern China as a prototype of idealized estuary. The Modaomen Estuary is one of the major outlets for the water discharge of the Pearl River, which is the main freshwater source of the Guangdong-Hong Kong-Macao Greater Bay Area. Due to seasonal variations in river discharge, the river experiences seasonal changes in the mean water discharge: 11000 m<sup>3</sup>/s from May to September and 3500 m<sup>3</sup>/s from November to February (Gong et al., 2022b). Additionally, the Modaomen Estuary is a microtidal estuary with irregular mixed semidiurnal tides, with the mean tidal height being 0.87m. In this region, saline water intrusions mainly occur in the dry seasons, due to the lower water discharge; this phenomenon threatens the freshwater supply to large cities, including Macau, Zhuhai, and Zhongshan. Saline water intrusion has been analyzed in several previous studies (Gong and Shen, 2011; Liu et al., 2014; Lin et al., 2019; Gong et al., 2022a, b), however, these studies mainly focused on the impact of external dynamic forcings (such as riverine discharge, tide, and wind) on saline water intrusion. The Modaomen Estuary has a complicated morphological structure, and its bathymetry is continually evolving since the 1960s; notably, the region is characterized by channel branching (Tan et al., 2019). Note that channel branching is a common occurrence in estuaries around the world (e.g. Yellow River estuary, Yangtze River estuary, Rhine-Meuse river delta). Therefore, the region is an ideal site for examining the impacts of channel branching on saline water intrusion in estuaries. Furthermore, the idealized model is a useful method to conduct a complex research question with a key concern, for example, Biemond et al. (2025) used an idealized model to explore the characteristics of salt intrusion in complex estuarine networks and revealed that the salt transport mechanisms within the network varied significantly, owing to the differences in the water depth, discharge, and tidal current phasing. In this study, we constructed an idealized estuary model as a prototype of Modaomen estuary to represent similar estuaries across the world. The main objectives of our study were to explore the impacts of channel branching on the saline water intrusion in estuaries and reveal the influencing mechanisms. Our study can improve the understanding of the cause of accelerated saline water intrusion in river deltas within the context of global changes and presents scientific guidelines for the sustainable management of coastal areas and river deltas.

## 2 Study area

#### 2.1 Hydrological characteristics

The Pearl River is the second-largest river in China, with a total length of 2,320 km and a drainage area of approximately 440,000 km<sup>2</sup>; it has an annual runoff of over 349.2 billion m<sup>3</sup> (Huang and Zhang, 2004). It comprises several tributaries, such as Xijiang, Beijiang, and Dongjiang, which contribute 77%, 15%, and 8% of the river flow, respectively (Wu et al., 2016a). These three major tributaries converge in the Pearl River Delta (Figure 1), forming a



complex network of waterways characterized by crisscrossing channels and a dense river network, before flowing into the sea through eight outlets. The Modaomen Estuary, located in the lower reaches of the Xijiang River, is the largest of the eight outlets, carrying approximately 28.3% of the total runoff of the Pearl River (Tan et al., 2019); it serves as an important freshwater source for the Guangdong-Hong Kong-Macao Greater Bay Area, providing freshwater to over 10 million people in nearby cities, such as Jiangmen, Zhongshan, Macao, and Zhuhai.

# 2.2 Evolution of channel branching in mouth bar area

Morphological changes of the mouth bar in the Modaomen Estuary occurred since the 1990s. Figures 2a-d shows a planar distribution map at the 4m isobath of the bar to depict the changes in mouth bar since the 1990s, and the isobaths deeper than 4m represented the channels of mouth bar. It is clear that the entire mouth bar had only one single channel in 1983; however, the bar at the Modaomen Estuary started to branch in 1994, and by 2000, the two branches gradually developed with channel widening. With the formation of the east branch, by 2005, the main branch was separated from the east and west shoals. The three shoals and two branches system of the Modaomen Estuary bar were thus formed. According to the previous studies (He et al., 2018; Tan et al., 2019), the channel branching was mainly caused by riverine discharge, especially for riverine flood. Regarding the mouth-bar body, it is clear that channel branching gradually occurred with bar crest moving towards sea and its height lowering from 1983 to 2005

(Figure 2e), which would influence the hydrodynamic structure in the Modaomen estuary.

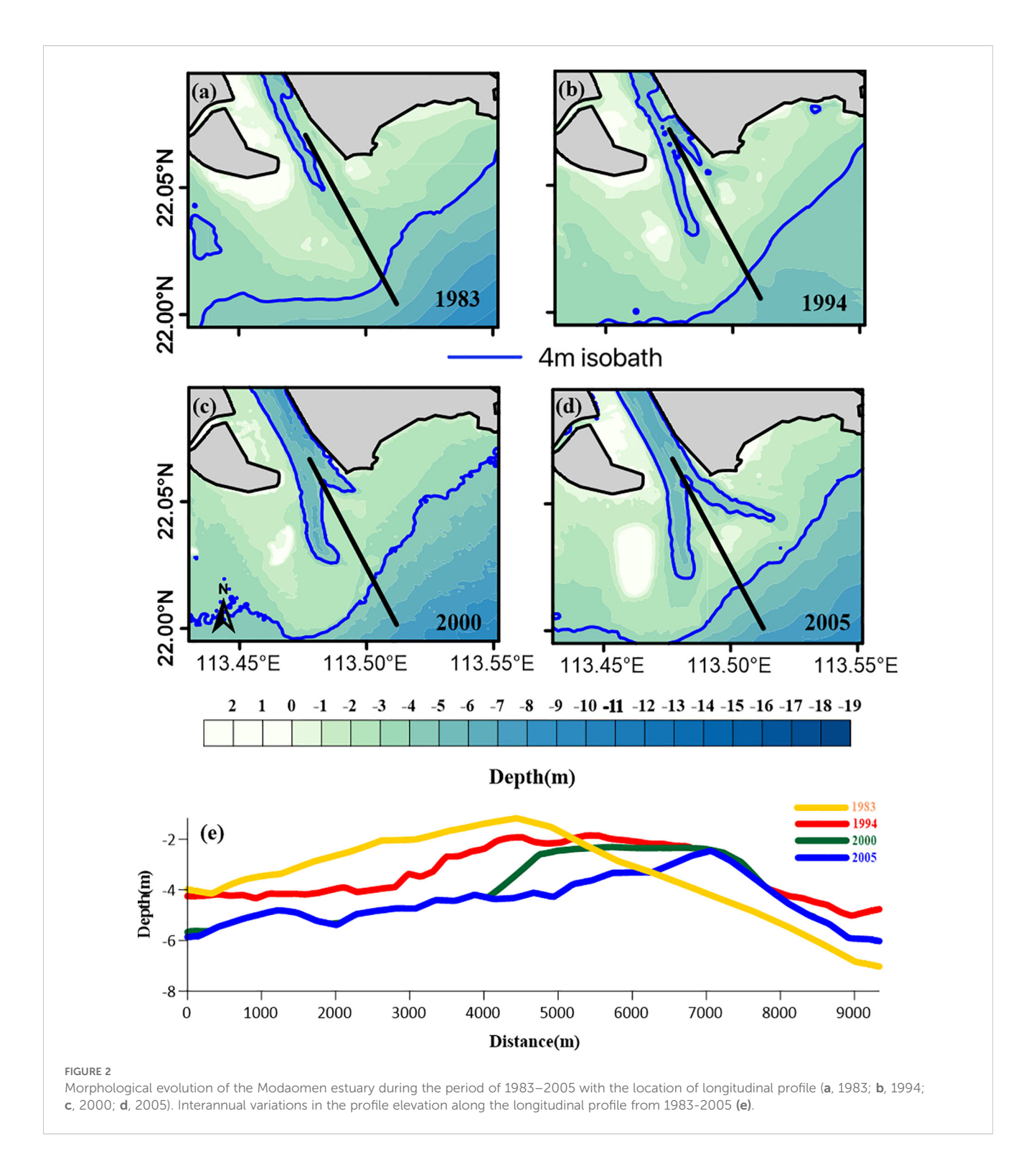
#### 3 Methods

# 3.1 Description of the idealized model developed in this study

#### 3.1.1 Delft3D model

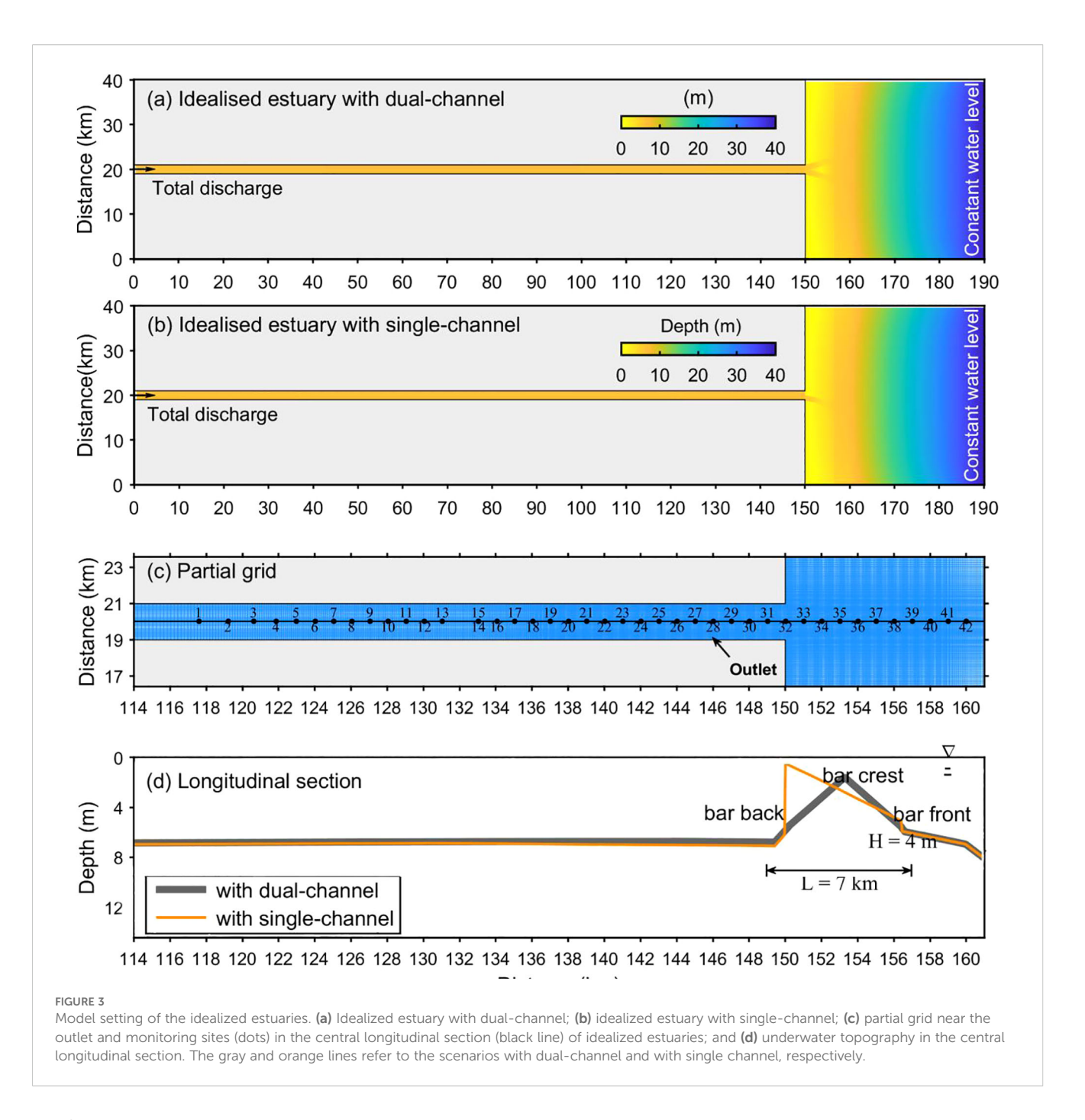
The Delft3D software, developed by the Deltares Institute in the Netherlands, is an integrated suite of software modules that encompass hydrodynamics, sediment transport, and marine environmental processes. It enables both two- (2D) and three-dimensional (3D) simulations. The model can simulate diverse coupled physical and ecological processes, including hydrodynamic processes, sediment transport, and water quality. Its flexible grid system and modular design render it effective for conducting simulations for complex topographical and dynamic conditions. Based on shallow-water equations, Delft3D can efficiently simulate hydrodynamic and mass transport processes driven by coupled factors, such as tides, waves, wind, and river discharge. The model is widely applied in studies on estuarine saltwater intrusion, pollutant dispersion, and sediment deposition (Deltares, 2025).

Furthermore, the Delft3D model demonstrates exceptional applicability and reliability for salinity simulations. Its coupled hydrodynamic and salinity transport modules can accurately simulate the formation of saltwater wedges, vertical salinity stratification, and salt-dispersion processes driven by tidal forcings



(Ruiz-Reina and López-Ruiz, 2021). By dynamically calculating the spatial salinity distributions in a region, the Delft3D model captures the combined effects of tides, river discharge, and morphological changes on saline water intrusion; thus, the model is suitable for studying the characteristics of saltwater intrusion in an estuarine environment. Moreover, the Delft3D model supports multiple boundary condition settings (Lesser et al., 2004; Deltares, 2025),

such as tidal harmonic constants and time-series river discharge inputs, facilitating the simulations of seasonal variations in river water salinity and the regulatory effects of morphological evolution on water salinity distribution across the river. Thus, the Delft3D model is widely recognized as an ideal tool for investigating estuarine saltwater intrusion, salt flux decomposition, and water-supply security assessments.



#### 3.1.2 Idealized model of Modaomen Estuary

Based on the Delft3D numerical model, considering the estuary's geometric characteristics as shown in Figure 3, in this study, we constructed a 3D idealized numerical model for the Modaomen Estuary in the Pearl River Delta. The computational domain of the idealized Modaomen Estuary was set as a rectangular area and included both the riverine and estuarine regions. To ensure the accuracy and stability of the model calculations, the upstream river boundary was placed outside the tidal influence zone (150km from the river mouth) to avoid tidal wave interference. The river-channel length and width were set to 150 and 2km, respectively, and the estuarine region was represented as a square structure of 40km ×

40km. The model employed a structured orthogonal curvilinear grid with varying density and resolution. The total number of grids was 123,904. The sea boundaries were set as the left, bottom, and right boundaries. The highest resolution of  $50m \times 50m$  was applied at x=150km near the river mouth, and the lowest resolution of  $400m \times 500m$  was used near the sea boundary. The x and y axes were set parallel and perpendicular to the coastline, respectively. In the 3D model, the vertical water column was divided into 10 layers using a  $\sigma$ -coordinate system, and the vertical mixing was calculated using the kepsilon (k- $\epsilon$ ) turbulence model. The bathymetric data for the idealized model were highly simplified based on the measured bathymetric data of the Modaomen Estuary. The simulation period

was 61 days; the salt dynamics in the idealized estuary adjusted quickly, reaching a near quasi-equilibrium state within 10 days.

The model focused on saltwater intrusion during the dry season. A total of 42 observation points was established along the central axis of the model to monitor the key parameters, with additional measurements conducted along the vertical section near the estuary mouth. The simulations on Days 46 and 53 were used to represent the simulation scenarios.

To analyze and evaluate the impact of the evolution of the outer channel of the Modaomen Estuary on the saltwater intrusion in the region, we considered two terrain scenarios (Scenarios 1 and 2) under identical hydrodynamic conditions. Scenario 1 represented an idealized dual-channel estuary, and scenario 2 represented an idealized single-channel estuary. Considering the morphological evolution of actual terrain data shown in Figure 2e during 1994-2005, the terrain data in two scenarios was designed as shown in Figure 3. The initial conditions, including the tidal current and salinity, were set to zero. The upstream river boundary was defined by a total discharge of 2,500 m<sup>3</sup>/s, lower than mean multiple-year value in the dry season, which was favored to the occurrence of saline water intrusion (Gong et al., 2022a). The water salinity at the river boundary and constant water levels were determined based on the astronomic tidal amplitudes and the phases of eight primary tides (M2, S2, N2, K2, Q1, K1, O1, and P1), which were obtained by data assimilation (Liu et al., 2016).

#### 3.2 Salt flux decomposition

The mechanism of saltwater intrusion in estuaries can be decomposed into three key components: advection transport driven by river discharge, steady shear dispersion caused by estuarine circulation, and tidal oscillatory transport resulting from tidal asymmetry (Gong et al., 2022b). The salt flux decomposition method is widely used to investigate the mechanisms of salt transport. In this study, we adopted the method proposed by Lerczak et al. (2006), wherein the tidally averaged salt flux (Fs) is decomposed into three parts (based on different driving forces): steady shear dispersion ( $F_E$ ), which is caused by estuarine circulation; tidal oscillatory salt flux ( $F_T$ ), which is driven by tidal asymmetry; and advection ( $F_R$ ), which results from river discharge. These parameters can be expressed as follows (Equations 1–4):

$$F_{S} = \left\langle \int usdA \right\rangle \tag{1}$$

$$\varphi_0 = \frac{1}{A_0} \left\langle \int \varphi dA \right\rangle \tag{2}$$

$$\varphi_E = \left\langle \frac{h + \eta}{h} \varphi \right\rangle - \varphi_0 \tag{3}$$

$$\varphi_T = \varphi - \varphi_0 - \varphi_E \tag{4}$$

where  $\varphi$  represents either the velocity u or salinity s, and  $A_0$  denotes the tidally averaged cross-sectional area. Thus, Fs can be

expressed as follows:

$$F_{S} = \left\langle \int (u_0 + u_E + u_T)(S_0 + S_E + S_T) dA \right\rangle$$

$$= \left\langle \int (u_0 S_0 + u_E S_E + u_T S_T) dA \right\rangle$$

$$= F_R + F_F + F_T$$
(5)

As this study focused on the salt flux per unit width of the cross-section, the cross-sectional width was set to a unit width. Thus, the Equation 5 can be rewritten as follows (Equations 6-10):

$$F_S = \left\langle \int usdh \right\rangle \tag{6}$$

$$\varphi_0 = \frac{1}{h_0} \left\langle \int \varphi dh \right\rangle \tag{7}$$

$$\varphi_E = \left\langle \frac{h + \eta}{h} \varphi \right\rangle - \varphi_0 \tag{8}$$

$$\varphi_T = \varphi - \varphi_0 - \varphi_E \tag{9}$$

$$\begin{split} F_S &= \left\langle \int (u_0 + u_E + u_T)(S_0 + S_E + S_T) dh \right\rangle \\ &= \left\langle \int (u_0 S_0 + u_E S_E + u_T S_T) dh \right\rangle \\ &= F_R + F_E + F_T \end{split} \tag{10}$$

where  $\langle \cdot \rangle$  denotes the tidal period average,  $h_0$  is the tidally averaged water depth, h is the depth below the mean sea level, and  $\eta$  represents the water-level fluctuation.

Based on the discretization of cross-sectional data (as described in the literature), the formula can be further rewritten as follows (Equations 11–17):

$$F_S = \left\langle \sum_{i=1}^n u_i S_i h_i \right\rangle \tag{11}$$

$$Q_f = \left\langle \sum_{i=1}^n u_i h_i \right\rangle \tag{12}$$

$$S_0 = \frac{1}{\mathbf{h}_0} \left\langle \sum_{i=1}^n S_i h_i \right\rangle \tag{13}$$

$$u_{E_i} = \left\langle \frac{h_i + \eta}{h_i} u_i \right\rangle - \frac{1}{h_0} Q_f \tag{14}$$

$$S_{E_i} = \left\langle \frac{h_i + \eta}{h_i} S_i \right\rangle - S_0 \tag{15}$$

$$u_{T_i} = u_i - u_{E_i} - \frac{1}{h_o} Q_f \tag{16}$$

$$S_{T_i} = S_i - S_{E_i} - S_0 (17)$$

where i represents the index of each layer in the unit-width cross-section;  $u_i$ ,  $S_i$ , and  $h_i$  denote the instantaneous velocity,

salinity, and water depth at the grid point corresponding to each layer, respectively; and  $Q_f$  is the tidally averaged river discharge.

The advection transport was driven by river discharge, resulting in the transport of salt from the estuary to the sea, denoting that the direction of salt transport was outward from the estuary to the sea. In contrast, the direction of shear dispersion and tidal oscillatory salt flux was from the open sea into the estuary. The shear dispersion caused by estuarine circulation was primarily related to the vertical gradients of salinity and velocity. The more pronounced the salinity stratification and the stronger the vertical circulation, the greater the shear dispersion salt flux. Note that salinity stratification itself was influenced by the tidal strength; when the tidal amplitude increased, the water mixing process was more uniform, resulting in a decrease in the shear dispersion salt flux. The tidal oscillatory salt flux, caused by the asymmetry between the flood and ebb tidal amplitudes, was mainly associated with the tidal amplitude. The larger the tidal amplitude, the greater the tidal oscillatory salt flux.

#### 4 Results

# 4.1 Changes in the extent (length) of saline water intrusion

The mean salinity values along the longitudinal profile during the spring and neap tides in different conditions are shown in Figure 4. The saline-water intrusion length was longer during the neap tide than during the spring tide in both the single and double channels, depicting agreement with the results of previous studies (Gong et al., 2022b). However, the lengths of saline water intrusion in single and double channels showed different patterns. During spring tide, the intrusion length of one isohaline in the bottom water layer reached 8.6km in the single channel 16km in the double channel; other isohalines also showed similar patterns. During the neap tide, the intrusion length of one isohaline in the bottom water layer was 26km in the single channel and 24.3km in the double channel, denoting changing tendency similar to those noted for other isohalines. Therefore, we could conclude that during the neap tide, the saline water intrusion in the double channel was more extensive than that in the single channel; the opposite phenomenon was observed during the spring tide.

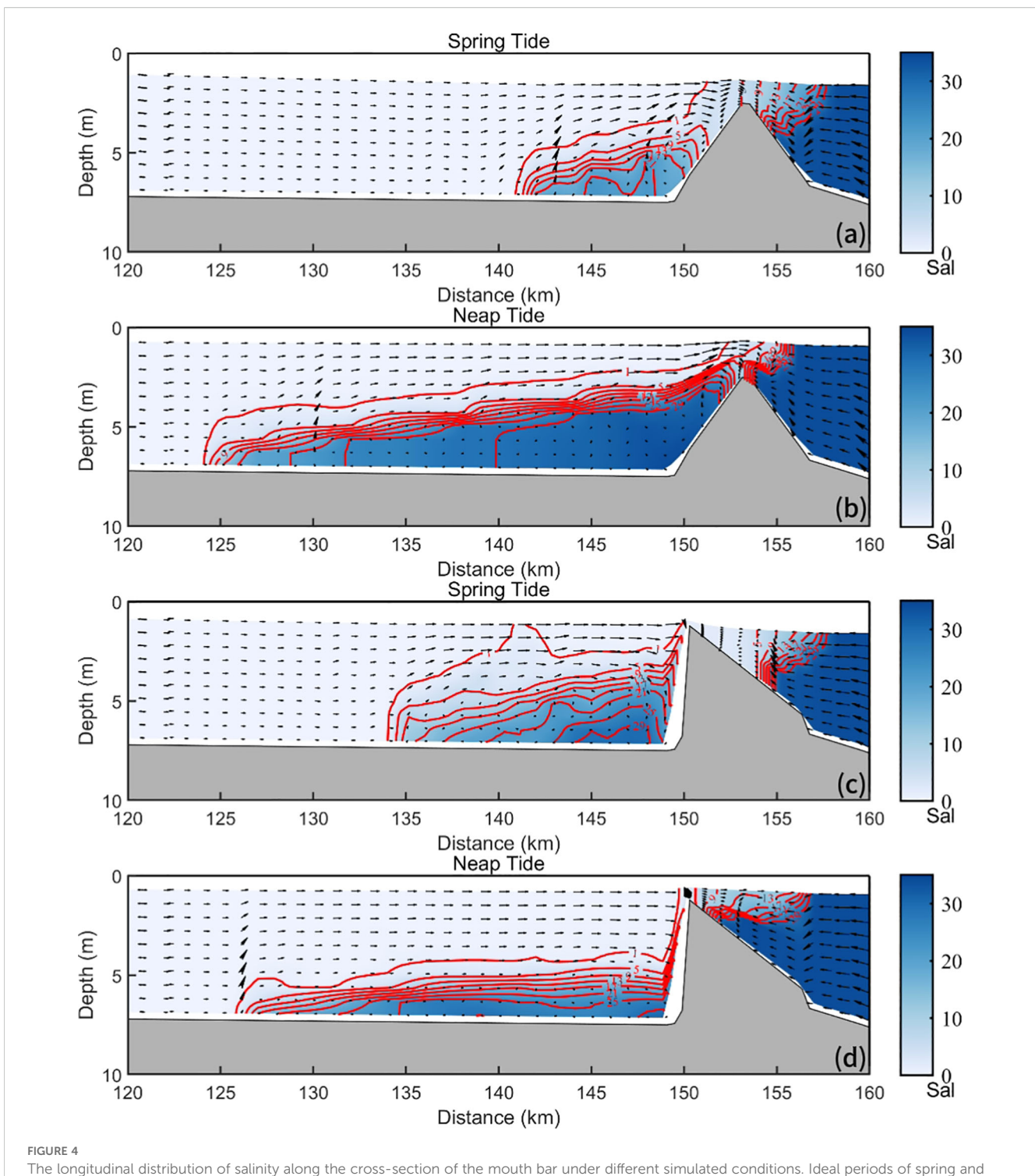
#### 4.2 Changes in salt flux

We calculated the salt flux per width unit along the longitudinal profile during the spring and neap tides. As shown in Figure 5, the salt flux generally depicted an increasing tendency from upstream to the outlets (along the longitudinal profile). Negative salt flux occurred closer to the upstream areas during neap tide than during spring tide. In addition, during the spring tide, the value of salt flux switched to negative at a distance of 128 and 132km from the upstream area in the single and double channels, respectively.

Furthermore, the salt flux toward land in the single channel was higher than that in the double channel (at the same site); for example, at a distance of 149km from the upstream area (i.e. at the outlet), the salt flux was  $49.63~{\rm psu\cdot m^2\cdot s^{-1}}$  in the single channel and  $34.19~{\rm psu\cdot m^2\cdot s^{-1}}$  in the double channel. Compared with the salt flux in the single channel during the neap tide, the negative value of salt flux occurred closer to the upstream area in the double channel, and the salt flux towards land was higher in the double channel at the same sites.

# 4.3 Changes in salt transport flux components

In this study, salt flux was mainly decomposed into three components: advective, steady shear, and tidal oscillatory, to reveal the mechanism of saline water intrusion. As shown in Figure 6, the advective component of salt flux showed positive values inside the outlets, indicating that the salt flux was towards the sea; outside the outlets, the component values were negative, indicating that the salt flux was towards the land. The steady shear dispersion and of tidal oscillatory components generally showed negative values, indicating that the salt flux was towards the land; compared with the landward salt flux, the values of these components during neap tide were larger than those noted during spring tide, which was the main cause for the longer intrusion distance of saline water during the neap tide. In addition, the salt flux caused by steady shear dispersion was generally higher than that caused by tidal oscillation in all conditions, with the only exception noted in the double channel during the spring tide. For example, in the single-channel estuary, during the spring tide, the salt flux caused by steady shear dispersion was higher only from Station 17 to Station 29; during neap tide, the values in the region from the estuary entrance (upstream) to Station 8 were high under both the conditions. Furthermore, the salt flux caused by steady shear dispersion along the longitudinal river profile depicted an increasing tendency from the upstream area to the outlet (with higher values observed at the outlets) but a decreasing tendency from the outlet to the sea. In the double-channel estuary, the decay rate of salt flux was relatively slow. During the spring tide, the steady shear flux gradually decayed after passing Station 32, decreasing to nearly 0 psu·m<sup>2</sup>·s<sup>-1</sup> at Station 37. During the neap tide, after reaching a peak value of approximately 65 psu·m<sup>2</sup>·s<sup>-1</sup> at Station 32, the steady shear flux depicted a steady decline, decreasing to 0 psu·m<sup>2</sup>·s<sup>-1</sup> at Station 40. In the single-channel estuary, the steady shear flux exhibited an exponential decay pattern after passing the estuary mouth. During spring tide, the steady shear flux value at Station 32 was about 21 psu·m<sup>2</sup>·s<sup>-1</sup> but decayed to almost 0 psu·m<sup>2</sup>·s<sup>-1</sup> at Station 33; the value remained 0 psu·m²·s⁻¹ thereafter. During the neap tide, the value at Station 32 (close to 42 psu·m<sup>2</sup>·s<sup>-1</sup>) was higher than that observed during the spring tide; similar to the observations during the spring tide, the value during the neap tide decreased to nearly 0 psu·m<sup>2</sup>·s<sup>-1</sup> at Station 33. However, during the neap tide, after Station 33, the flux increased to around 3-5 psu·m<sup>2</sup>·s<sup>-1</sup> between Stations 35 and 38, with the value finally decreasing to 0 psu·m<sup>2</sup>·s<sup>-1</sup> at Station 39.



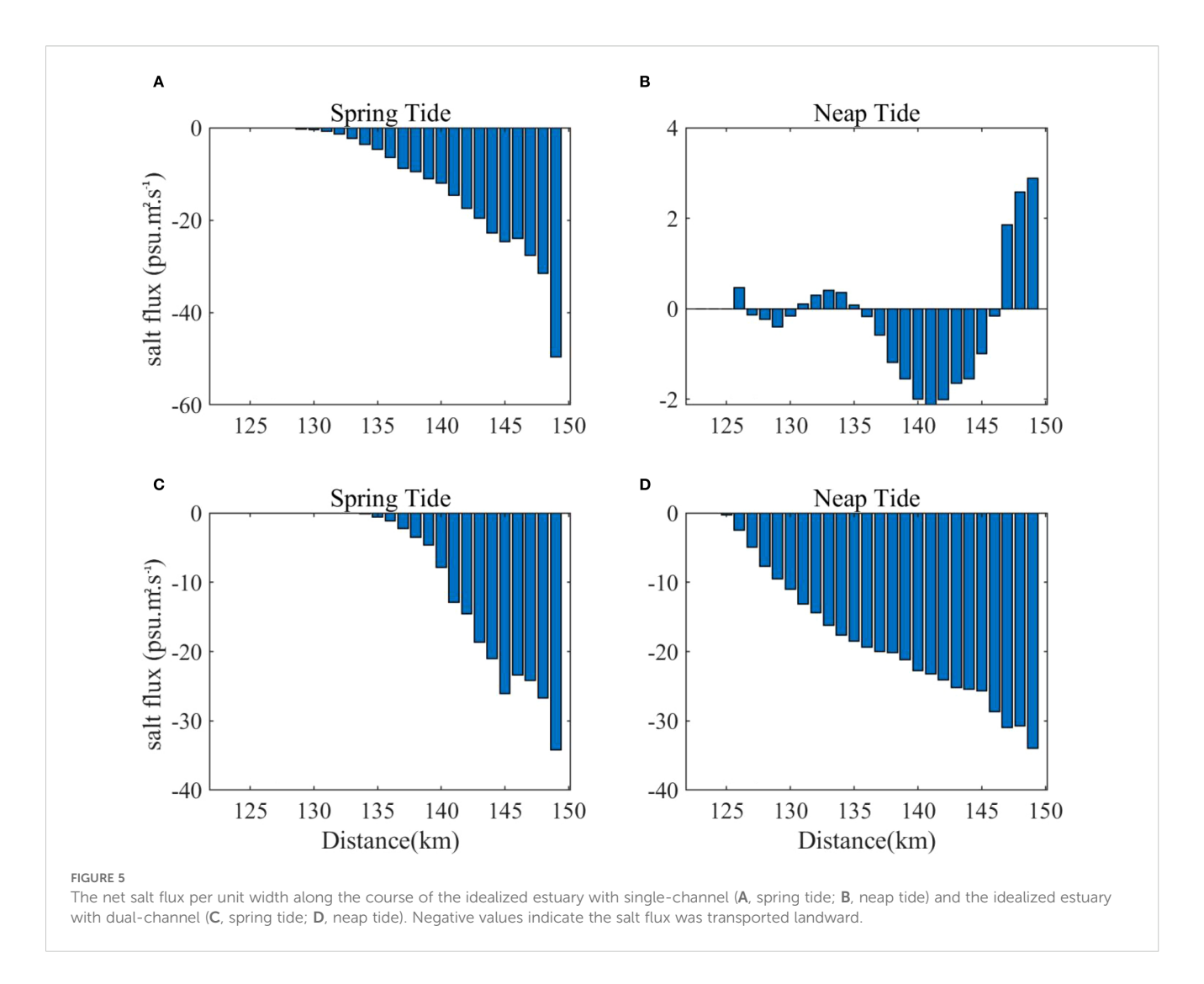
The longitudinal distribution of salinity along the cross-section of the mouth bar under different simulated conditions. Ideal periods of spring and neap tides at double-channel estuaries (a, b) and ideal periods of spring and neap tides at single-channel estuaries (c, d). The red contour lines represent salinity. The black arrow indicates ocean currents, and the one to the right indicates the direction from the river channel to the open sea

#### 5 Discussion

### 5.1 Impact of channel branching

The results indicated that the extent of saline water intrusion was greatly influenced by the morphological structure of the

Modaomen Estuary. In particular, the salt transport processes in the region were mainly determined by the estuarine dynamic structure (e.g. estuarine circulation and tidal asymmetry), as indicated by the decomposition of the salt flux component. Several previous studies reported the effects of morphological evolution on the estuarine dynamic structure; for example,



Zhang et al. (2023) reported that the substantial loss in the intertidal areas with changing geometry (from a highly-curved bank to a highly constrained channel) weakened the flood tidal asymmetry of the north branch in the Yangtze Estuary. Therefore, we examined the changes in the dynamic structure in the Modaomen Estuary under different simulated conditions to reveal the influencing mechanism of channel branching.

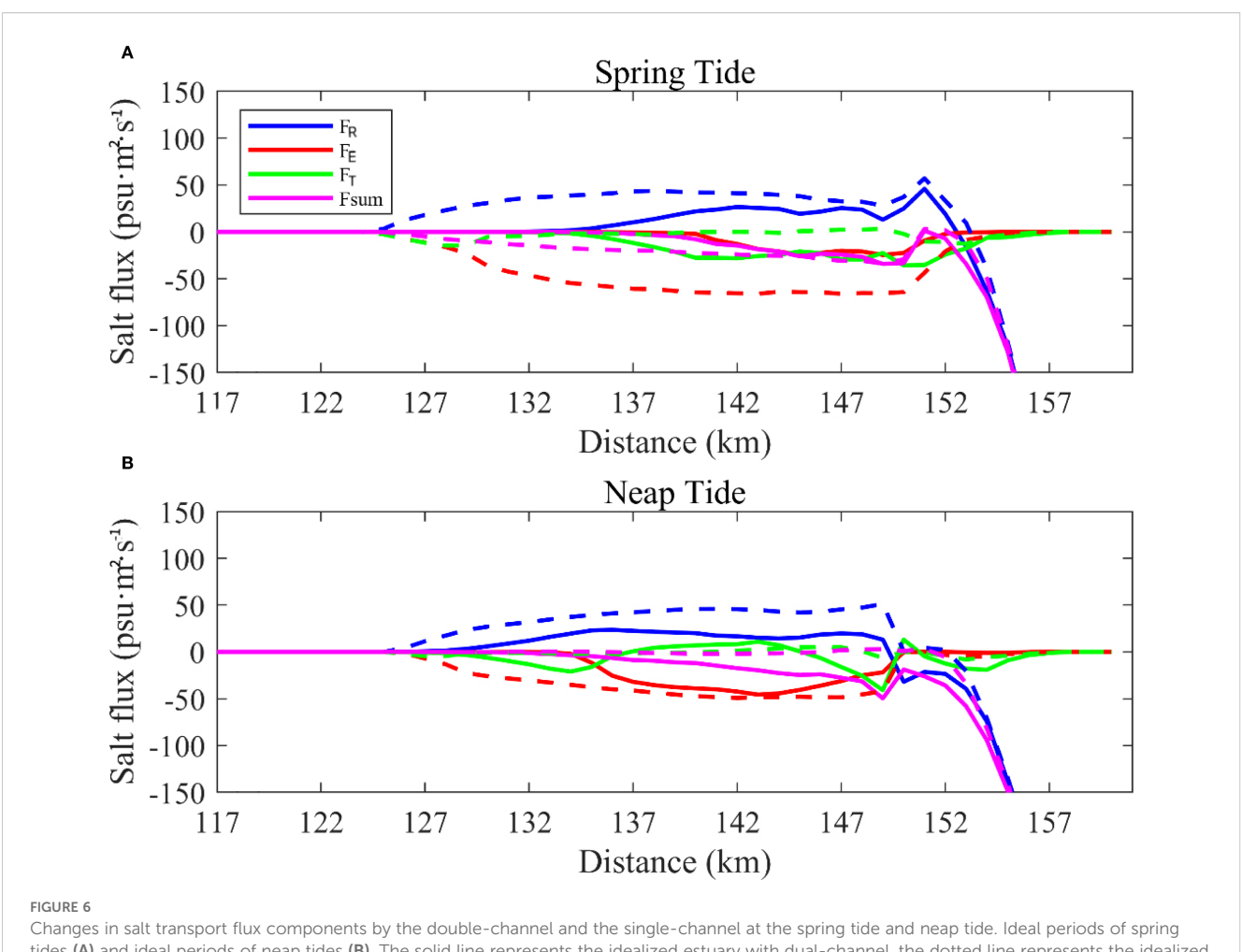
#### 5.1.1 Blocking water effects

Mouth bars generally develop in estuaries; therefore, their morphology is complicated. In particular, they serve as a sill that affects the exchange flow between the estuary and ocean (Gong et al., 2022b). According to Gong et al. (2022b), mouth bars can weaken saltwater intrusion in estuaries by 15–23%. Saline water, accompanied by flood currents, can intrude the inner estuary region. In this study, the intruded saline waters were retained during the neap tide, in response to the blocking effects of the mouth bar. The mouth bar exerted a substantial effect on blocking the intruded saline waters and increasing the retention time of the intruded water. Figure 7 shows the salinity distribution along the longitudinal profile at the ebb slack during the spring and neap

tides. The saline waters were retained over longer distances across the estuary during the neap tide, compared to the retention extent of the saline water intrusion observed during the spring tide. In the simulation, the mouth bar formed in the single-channel simulation was steeper than that formed in the double-channel simulation. During the spring tide, the saline waters were retained over longer distances across the estuary, with a single channel compared with a double channel; the opposite pattern was observed during the neap tide. Furthermore, high salinity was limited to the bottom water layers in the single channel while depicting higher salinity stratification compared with that noted in the double channel.

#### 5.1.2 Impact of estuarine circulation

The simulation conducted in this study revealed that estuarine circulation played an important role in the extent of saline water intrusion; for example, the intensification of estuarine circulation markedly amplified both the strength and spatial asymmetry of saltwater intrusion. Zhu et al. (2003) conducted idealized numerical experiments of an estuary and revealed that the baroclinic gradient generated by the salinity front caused a landward density current in the bottom layer; then, for ensuring mass conservation, a



Changes in salt transport flux components by the double-channel and the single-channel at the spring tide and neap tide. Ideal periods of spring tides (A) and ideal periods of neap tides (B). The solid line represents the idealized estuary with dual-channel, the dotted line represents the idealized estuary with single-channel. In the figures,  $F_R$ ,  $F_E$  ad  $F_T$  represents the item of advective, steady shear and for tidal oscillatory, respectively. Negative values indicate the salt flux was transported landward.

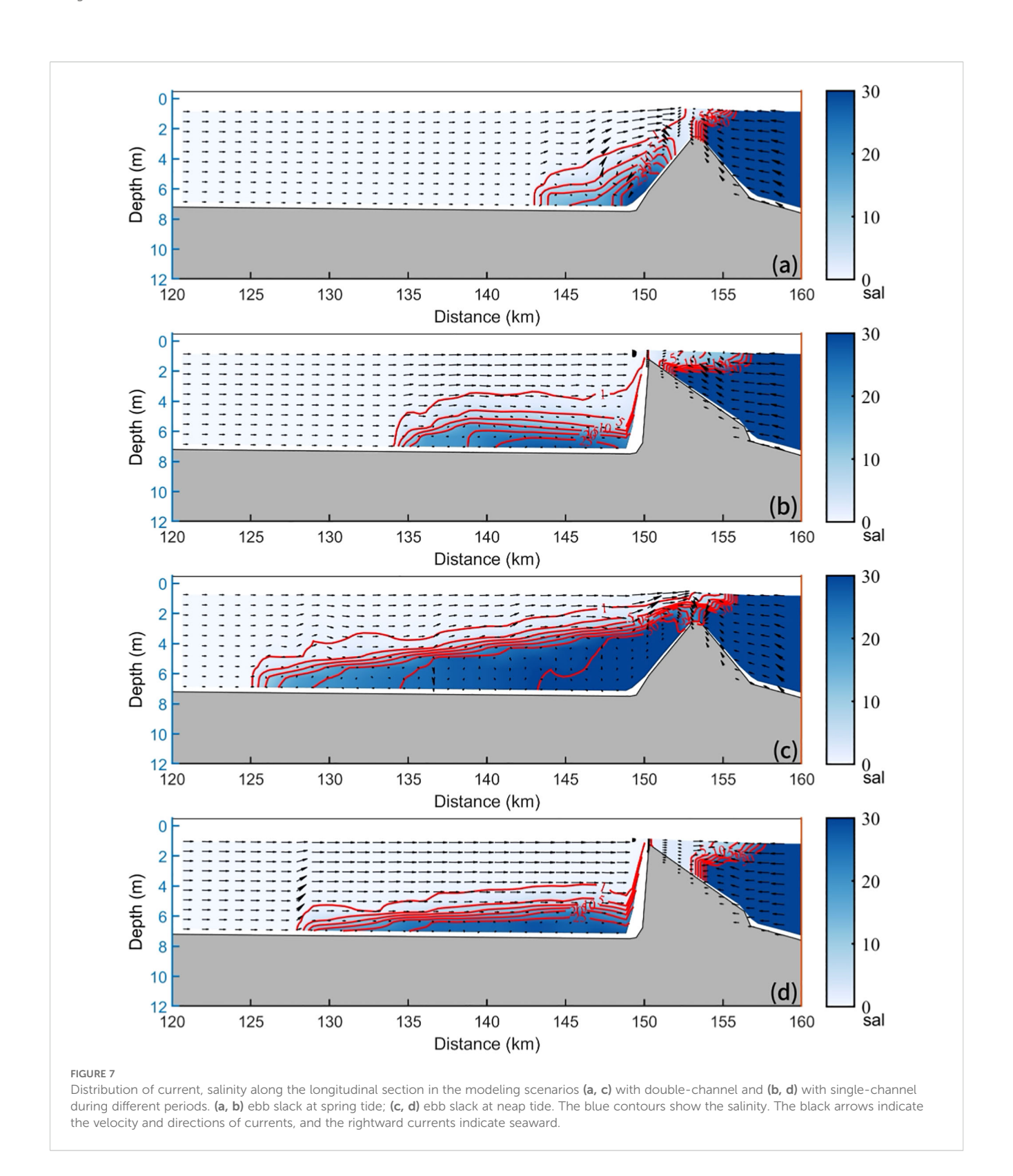
synchronous increase occurred in the seaward surface current, resulting in a longitudinal residual circulation pattern. When the baroclinic effect strengthened—for example, as the intensity of saltwater intrusion increased—the bottom density current accelerated, leading to a pronounced landward extension of the saline waters, with the penetration in the bottom water layer being roughly 3% greater than that in the surface layer.

We calculated the residual currents in different simulated conditions to determine the dynamic structure of estuarine circulation in the study region (Figure 8). During the spring tide, double estuarine circulation was detected in both the single and double channels; however, we noted significant differences in the spatial distribution of estuarine circulation between the single and double channels. For the double channels, the residual current flowed towards the sea, through the water column at Station 22, and towards the sea in the surface water layers but towards land in the bottom water layers at Station 22 with single channel. This indicated that the location of estuarine circulation was closer to the upstream area in the single channel, compared to that observed in the double channel, indicating higher intensity estuarine circulation in the single channel, which contributed to the greater extent of saline

water intrusion in the region. During the neap tide, we observed notable differences in the distribution of estuarine circulation between the single and double channels. Compared with the velocity of the residual current towards the land at Stations 22 and 30, the velocity in the bottom water layers was more pronounced in the double channel than in the single channel.

#### 5.1.3 Impact of tidal asymmetry

Previous studies analyzed the impacts of tidal asymmetry on riverine material transport, for example, Pham Van Bang et al. (2023) revealed that tidal asymmetry significantly influenced riverine material transport through turbulence modulation and phase-difference correction. In this study, we calculated the ratio of the flood and ebb currents during the spring and neap tides (Li et al., 2025), shown in Figure 9. The ratio in the surface water layer was less than 1, indicating ebb-dominance in the surface layer. However, the ratio in the bottom layer was greater than 1, indicating flood-dominance in the bottom layer. During the spring tide, the ratio was approximately 1 throughout the water column; during the neap tide, at a few stations (Stations 10, 22, 34, and 38), the ratio was higher than 1. This phenomenon indicated that the tidal asymmetry



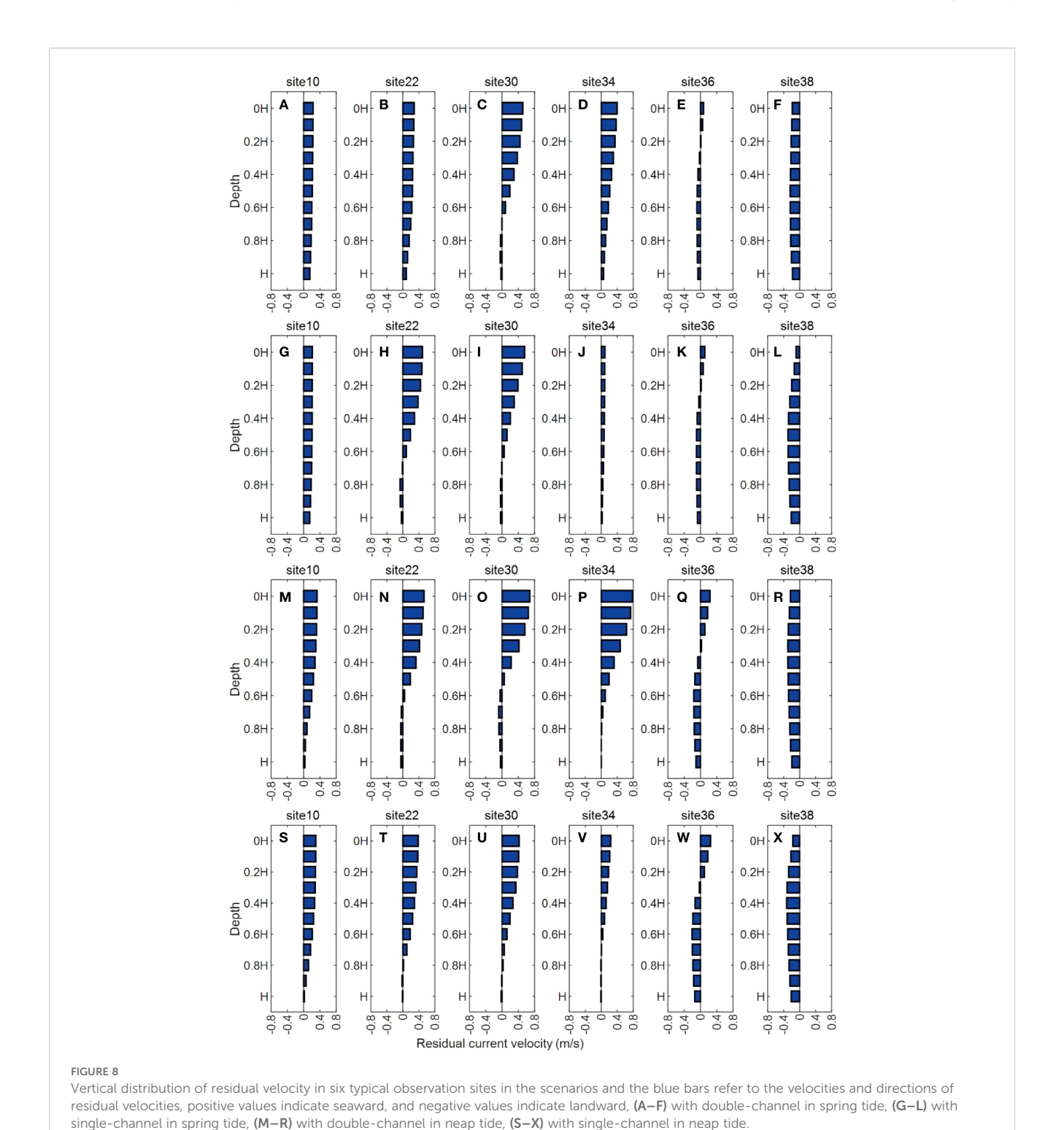
was pronounced during the neap tide, thereby increasing the intensity of the saline water intrusion in the region. Furthermore, the flood dominance occurred in regions that were located away from the estuary in double channel condition than single channel condition, contributing to the intensity of saline water intrusion in the region.

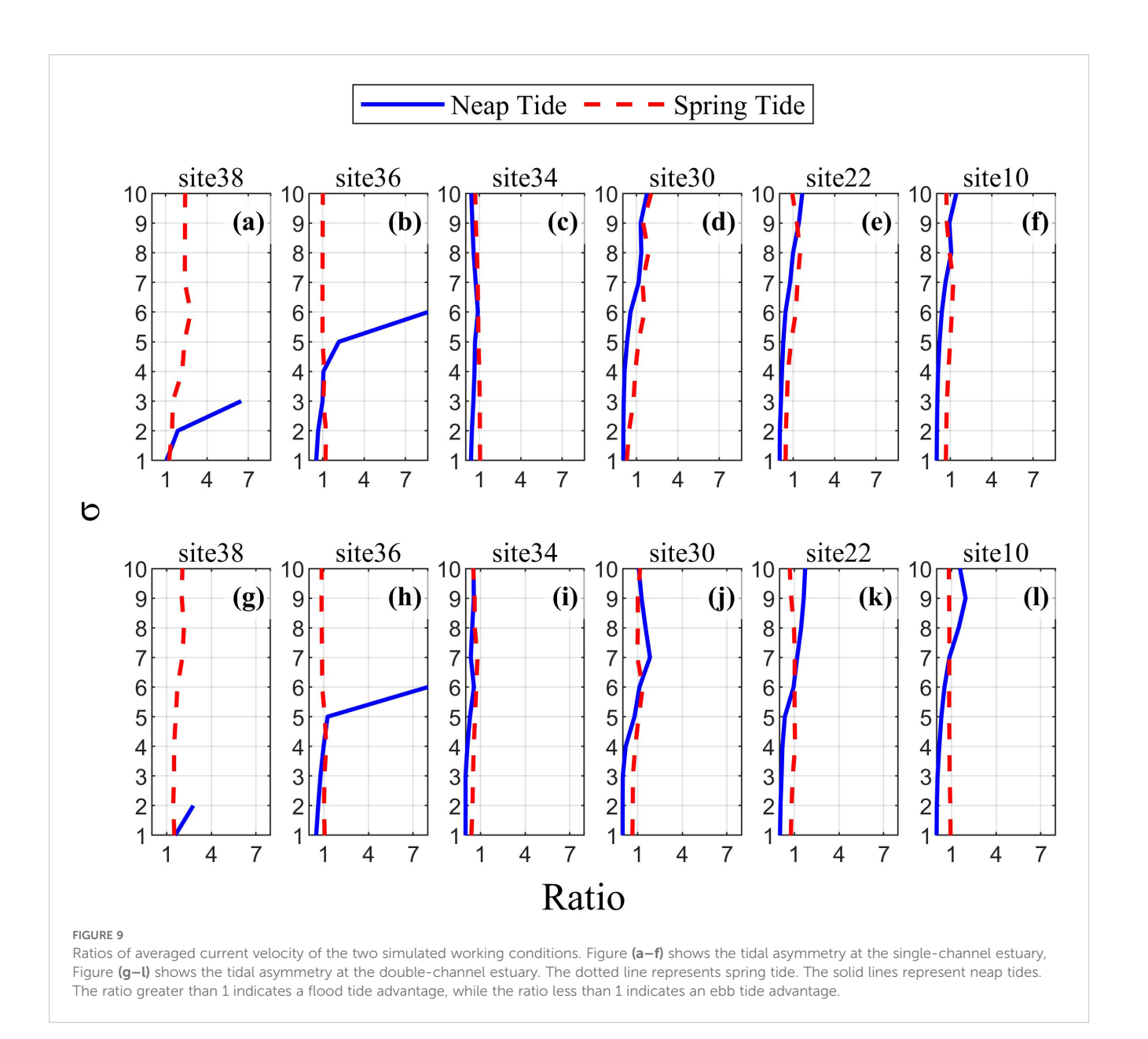
# 5.2 Study implications for estuarine management

The formation and evolution of mouth bar in the estuaries was affected by many factors, such as river discharge, tide, wave and sediment load (Edmonds and Slingerland, 2007; Leonardi et al.,

2013; He et al., 2018; Tan et al., 2019). And it can influence the estuarine dynamic, for example, Xie et al. (2017) indicated that the inside bar formation in the Qiantang Estuary caused the deformation of tidal wave and resulted in tidal asymmetry using an idealized numerical model. As results, morphological evolution influenced salinity intrusion processes in the estuaries and river deltas, such as the Yangtze River Estuary (Wu et al., 2016b), the lower Hudson River Estuary (Ralston and Geyer, 2019), Vietnamese

Mekong Delta (Binh et al.,2021). As indicated in this study, the morphological evolution of mouth bars resulted from channel branching exhibit various impacts on saline water intrusion, mainly by affecting the estuarine dynamics. Therefore, the effects of the morphological evolution of mouth bars on the water resources in estuaries must be investigated. In context of global changes, human activities exerted great effects on morphological evolution in the estuaries and river deltas, such as Qiantang Estuary





(Xie et al., 2021), Yangtze River Estuary (Luan et al., 2016), and Lingdingyang Bay of the Pearl River delta (Yang et al., 2019). Therefore, special attentions must be paid to sustainable management of river estuaries and deltas to ensure the freshwater resource safety.

#### 6 Conclusions

In this study, we explored the impacts of morphological changes in the mouth bar structure (caused by channel branching) on the saline water intrusion in the Modaomen Estuary by developing an idealized model of the region. The intensity of saline water intrusion was higher during the neap tide than during the spring tide in both the single- and double-channel simulations. Channel branching affected the saline water intrusion during both the spring and neap tides mainly by affecting the estuarine dynamics (e.g. estuarine

circulation and tidal asymmetry). During the neap tide, the extent of saline water intrusion in the double-channel simulation was more significant than that observed in the single-channel simulation; however, the opposite pattern was observed during the spring tide. This phenomenon was mainly caused by the changes in the salt transport mechanism, indicated by the decomposition of the salt flux component. In general, channel branching altered the circulation structure in the estuary, depicting enhanced estuarine circulation in the single- and double-channel simulations during the spring and neap tides, respectively. The mouth bar depicted a 'blocking effect' on the saline water intrusion and recession in the region; the retention of saline water in the single- and doublechannel simulations was pronounced during the spring and neap tides, respectively, thereby promoting estuarine circulation. Therefore, to ensure water security in estuaries, the morphological effects of estuarine regulation projects must be considered for effective estuarine management.

## Data availability statement

The original contributions presented in the study are included in the article/supplementary material. Further inquiries can be directed to the corresponding author.

#### **Author contributions**

PW: Formal analysis, Writing – original draft, Software, Visualization. LH: Methodology, Software, Writing – review & editing. JL: Writing – review & editing, Software, Methodology. HYL: Investigation, Writing – review & editing, Methodology. HWL: Methodology, Writing – review & editing, Software. CT: Writing – review & editing, Formal analysis, Methodology. HC: Methodology, Software, Writing – review & editing. FL: Supervision, Writing – review & editing, Writing – original draft.

## **Funding**

The author(s) declare financial support was received for the research and/or publication of this article. This research was financially supported by the Guangdong Provincial Talents Project (Grant No. 2023TQ07G828), Science and Technology Innovation Program from Water Resources of Guangdong Province (Grant No. 2025-20) and Fundamental Research Funds for the Central Universities, Sun Yat-sen University (Grant No. 24XKJC031).

#### References

Biemond, B., Kranenburg, W. M., Huismans, Y., de Swart, H. E., and Dijkstra, H. A. (2025). Dynamics of salt intrusion in complex estuarine networks: an idealised model applied to the Rhine-Meuse Delta. *Ocean Sci.* 21, 261–281. doi: 10.5194/os-21-261-2025

Binh, D. V., Kantoush, S. A., Sumi, T., Mai, N. P., Ngoc, T. A., Trung, L. V., et al. (2021). Effects of riverbed incision on the hydrology of the Vietnamese Mekong Delta. *Hydrological Processes* 35, 1–21. doi: 10.1002/hyp.14030

Costa, Y., Martins, I., de Carvalho, G. C., and Barros, F. (2023). Trends of sea-level rise effects on estuaries and estimates of future saline intrusion. *Ocean Coast. Manage.* 236, 106490. doi: 10.1016/j.ocecoaman.2023.106490

Deltares (2025). Delft3D-FLOW user manual. *Deltares, Version 4.05*. Available online at: https://content.oss.deltares.nl/delft3d4/Delft3D-FLOW\_User\_Manual.pdf (Accessed September 17, 2025).

Edmonds, D. A., and Slingerland, R. L. (2007). Mechanics of river mouth bar formation: Implications for the morphodynamics of delta distributary networks. *J. Geophysical Res.* 112, F02034. doi: 10.1029/2006JF000574

Gong, W., Lin, Z., Zhang, H., and Lin, H. (2022a). The response of salt intrusion to changes in river discharge, tidal range, and winds, based on wavelet analysis in the Modaomen Estuary, China. *Ocean Coast. Manage.* 219, 106060. doi: 10.1016/j.ocecoaman.2022.106060

Gong, W., and Shen, J. (2011). The response of salt intrusion to changes in river discharge and tidal mixing during the dry season in the Modaomen Estuary, China. *Continental Shelf Res.* 31, 769–788. doi: 10.1016/j.csr.2011.01.011

Gong, W., Zhang, G., Zhang, H., Yu, X., Zhu, L., and Li, S. (2022b). The effects of mouth bar on salt intrusion in a partially mixed estuary. *J. Hydrology* 612, 128261. doi: 10.1016/j.jhydrol.2022.128261

## **Acknowledgments**

The authors thank the editor and reviewers for their invaluable and constructive suggestions on our manuscript.

#### Conflict of interest

The authors declare that the research was conducted in the absence of any commercial or financial relationships that could be construed as a potential conflict of interest.

#### Generative AI statement

The author(s) declare that no Generative AI was used in the creation of this manuscript.

Any alternative text (alt text) provided alongside figures in this article has been generated by Frontiers with the support of artificial intelligence and reasonable efforts have been made to ensure accuracy, including review by the authors wherever possible. If you identify any issues, please contact us.

#### Publisher's note

All claims expressed in this article are solely those of the authors and do not necessarily represent those of their affiliated organizations, or those of the publisher, the editors and the reviewers. Any product that may be evaluated in this article, or claim that may be made by its manufacturer, is not guaranteed or endorsed by the publisher.

He, Y., Ye, R., Tang, C., and Yang, L. (2018). Relationship between the morphological evolution of the river mouth bar and fluvial input in the Modaomen Estuary. *Environ. Earth Sci.* 77, 668. doi: 10.1007/s12665-018-7856-x

Hlaing, N. O., Azhikodan, G., and Yokoyama, K. (2024). Effect of monsoonal rainfall and tides on salinity intrusion and mixing dynamics in a macrotidal estuary. *Mar. Environ. Res.* 202, 106791. doi: 10.1016/j.marenvres.2024.106791

Huang, Z., and Zhang, W. (2004). Impacts of artificial factors on the evolution of geomorphology during recent thirty years in the Zhujiang Delta. *Quaternary Sci.* 24, 394–401. (In Chinese with English abstract).

Leonardi, N., Canestrelli, A., Sun, T., and Fagherazzi, S. (2013). Effect of tides on mouth bar morphology and hydrodynamics. *J. Geophysical Research: Oceans* 118, 4169–4183. doi: 10.1002/jgrc.20302

Lerczak, J. A., Geyer, W. R., and Chant, R. J. (2006). Mechanisms driving the time-dependent salt flux in a partially stratified estuary. *J. Phys. Oceanography* 36, 2296–2311. doi: 10.1175/JPO2959.1

Lesser, G. R., Roelvink, J. A., van Kester, J. A. T. M., and Stelling, G. S. (2004). Development and validation of a three-dimensional morphological model. *Coast. Eng.* 51, 883–915. doi: 10.1016/j.coastaleng.2004.07.014

Li, X., Liu, F., Zou, H., Tan, C., Huang, J., Mo, S., et al. (2025). Longitudinal transport of net suspended sediment in the river-dominated Modaomen Estuary of the Pearl River: Effects of river, tide, and mouth bar. *Mar. Geology* 486, 107575. doi: 10.1016/j.margeo.2025.107575

Lin, Z., Zhang, H., Lin, H., and Gong, W. (2019). Intraseasonal and interannual variabilities of saltwater intrusion during dry seasons and the associated driving forcings in a partially mixed estuary. *Continental Shelf Res.* 174, 95–107. doi: 10.1016/j.csr.2019.01.008

Liu, B., Yan, S., Chen, X., Lian, Y., and Xin, Y. (2014). Wavelet analysis of the dynamic characteristics of saltwater intrusion -A case study in the Pearl River Estuary of China. *Ocean Coast. Manage.* 95, 81–92. doi: 10.1016/j.ocecoaman.2014.03.027

- Liu, R., Wang, Y., Gao, J., Wu, Z., and Guan, W. (2016). Turbidity maximum formation and its seasonal variations in the Zhujiang (Pearl River) Estuary, southern China. *Acta Oceanologica Sin.* 35, 22–31. doi: 10.1007/s13131-016-0897-7
- Luan, H. L., Ding, P. X., Wang, Z. B., Ge, J. Z., and Yang, S. L. (2016). Decadal morphological evolution of the Yangtze Estuary in response to river input changes and estuarine engineering projects. *Geomorphology* 265, 12–23. doi: 10.1016/j.geomorph.2016.04.022
- Luo, X. L., Zeng, E. Y., Ji, R. Y., and Wang, C. P. (2007). Effects of in-channel sand excavation on the hydrology of the Pearl River Delta, China. *J. Hydrology* 343, 230–239. doi: 10.1016/j.jhydrol.2007.06.019
- MacCready, P., and Geyer, W. R. (2010). Advances in estuarine physics. *Annu. Rev. Mar. Sci.* 2, 35–58. doi: 10.1146/annurev-marine-120308-081015
- Nguyen, A., Savenije, H., Pham, D., and Tang, D. (2008). Using salt intrusion measurements to determine the freshwater discharge distribution over the branches of a multi-channel estuary: The Mekong Delta case. *Estuarine Coast. Shelf Sci.* 77, 433–445. doi: 10.1016/j.ecss.2007.10.010
- Nicholls, R. J., and Cazenave, A. (2010). Sea-level rise and its impact on coastal zones. Science 328, 1517–1520. doi: 10.1126/science.1185782
- Pham Van Bang, D., Phan, N. V., Guillou, S., and Nguyen, K. D. (2023). A 3D numerical study on the tidal asymmetry, residual circulation and saline intrusion in the Gironde Estuary (France). *Water* 15, 4042. doi: 10.3390/w15234042
- Pokavanich, T., and Guo, X. (2024). Saltwater intrusion in Chao Phraya Estuary: A long, narrow and meandering partially mixed estuary influenced by water regulation and abstraction. *J. Hydrology: Regional Stud.* 52, 101686. doi: 10.1016/j.ejrh.2024.101686
- Ralston, D. K., and Geyer, W. R. (2019). Response to channel deepening of the salinity intrusion, estuarine circulation, and stratification in an urbanized estuary. *J. Geophysical Research: Oceans* 124, 4784–4802. doi: 10.1029/2019JC015006
- Ruiz-Reina, A., and López-Ruiz, A. (2021). Short-term river mouth bar development during extreme river discharge events: The role of the phase difference between the peak discharge and the tidal level. *Coast. Eng.* 170, 103982. doi: 10.1016/j.coastaleng.2021.103982
- Scully, M. E., and Friedrichs, C. T. (2007). Sediment pumping by tidal asymmetry in a partially mixed estuary. *J. Geophysical Res.* 112, C07028. doi: 10.1029/2006JC003784

- Simpson, J. H., Brown, J., Matthews, J., and Allen, G. (1990). Tidal straining, density currents, and stirring in the control of estuarine stratification. *Estuaries* 13, 125–132. doi: 10.2307/1351581
- Tan, C., Huang, B., Liu, F., Huang, G., Qiu, J., Chen, H., et al. (2019). Recent morphological changes of the mouth bar in the Modaomen Estuary of the Pearl River Delta: Causes and environmental implications. *Ocean Coast. Manage.* 181, 104896. doi: 10.1016/j.ocecoaman.2019.104896
- Wu, C. S., Yang, S., Huang, S., and Mu, J. (2016a). Delta changes in the Pearl River estuary and its response to human activities, (1954-2008). *Quaternary Int.* 392, 147–154. doi: 10.1016/j.quaint.2015.04.009
- Wu, S. H., Cheng, H. Q., Xu, Y. J., Li, J. F., and Zheng, S. W. (2016b). Decadal changes in bathymetry of the Yangtze River Estuary: human impacts and potential saltwater intrusion. *Estuarine Coast. Shelf Sci.* 182, 158–169. doi: 10.1016/j.ecss.2016.10.002
- Xie, D. F., Gao, S., Wang, Z. B., Pan, C. H., Wu, X., and Wang, Q. (2017). Morphodynamic modeling of a large inside sandbar and its dextral morphology in a convergent estuary: Qiantang Estuary, China. *J. Geophysical Research: Earth Surface* 122, 1553–1572. doi: 10.1002/2017JF004293
- Xie, D. F., Wang, Z. B., van der Wegen, M., and Huang, J. B. (2021). Morphodynamic modeling the impact of large-scale embankment on the large bar in a convergent estuary. *Mar. Geology* 442, 106638. doi: 10.1016/j.margeo.2021.106638
- Yang, L., Liu, F., Gong, W., Cai, H., Yu, F., and Pan, H. (2019). Morphological response of Lingding bay in the Pearl River estuary to human intervention in recent decades. *Ocean Coast. Manage.* 176, 1–10. doi: 10.1016/j.ocecoaman.2019.04.011
- Zhang, E., Gao, S., Savenije, H. H. G., Si, C., and Cao, S. (2019). Saline water intrusion in relation to strong winds during winter cold outbreaks: North Branch of the Yangtze Estuary. *J. Hydrology* 574, 1099–1109. doi: 10.1016/j.jhydrol.2019.04.096
- Zhang, M., Wu, H., Dai, Z., Mi, J., and Cai, H. (2023). Morphodynamic resilience of the tide-dominated estuary with interference from tidal flat reclamations. *J. Geophysical Research: Oceans* 128, e2022JC019321. doi: 10.1029/2022JC019321
- Zhu, J., Hu, S., and Fu, D. (2003). Estuarine circulation and saltwater intrusion I: Model and control numerical experiment. *J. Ocean Univ. Qingdao-Chinese Edition* 33, 180–184. W.H.
- Zhu, J., Wu, H., Li, L., and Qiu, C. (2018). Saltwater intrusion in the Changjiang Estuary. In Coastal environment, disaster, and infrastructure A case study of China's coastline. Edited by X.S. Liang and Y. Zhang. (IntechOpen). pp. 49–73.